A Neuro-Fuzzy Controlled Solar Photovoltaic and PHEV based Frequency Regulation in a Microgrid without Storage System

K. S. V. Phani Kumar and S. Venkateshwarlu

Dept. of Electrical and Electronics Engineering, C.V.R College of Engineering, Hyderabad, Telangana, India
E-mail: {phani5016; svip123}@gmail.com

Received 23 April 2017; Accepted 14 October 2017;
Publication 7 November 2017

Abstract

This paper proposes a distributed resource management scheme to avoid the need for energy storage and achieve the required frequency regulation. The energy sources considered in the microgrid are Solar PhotoVoltaics (SPV), Diesel Generators (DG), Fuel Cells (FC) and Plug-in Hybrid Electric Vehicles (PHEV). The frequency regulation is done by considering the SPV operation at a Limited-Power-Point (LPP) for spinning reserve using neuro-fuzzy control in coordination with PHEVs and other sources. In vehicle-to-grid (V2G) mode, State of Charge (SOC) of the battery in a PHEV shall be the deciding factor in allowing it to participate in the regulation. A simple additive-adaptive strategy based algorithm is proposed and tested in the isolated microgrid environment. Satisfactory results of frequency regulation were obtained upon consideration of scenarios, varying the load and insolation in steps.

Keywords: Neuro-Fuzzy control, Frequency regulation, Energy management, Limited-power-point-tracking, Solar PV, Fuel cells, V2G, Power quality.

Journal of Green Engineering, Vol. 7, 311–332.
doi: 10.13052/jge1904-4720.71213

1 Introduction

In a decentralized power system, where independent power producers are producing power with generation sources available locally, the integrated operation has been a critical issue for the power engineers. New concept called power-on-wheels has come up in the energy market where, PHEV get their batteries charged at the domestic household or at commercial places like offices, parking lots using dedicated energy sources like SPV, FC or grid connection through a charge controller [1]. These vehicle batteries containing enough SOC are eligible for pumping power into the grid at the power stations meant for V2G or Grid-to-Vehicle (G2V) connections. Whenever there is a need for frequency regulation, PHEVs can be called for participation in load sharing. Due to the ease of transportation, the vehicles can be connected close to the loads so that transmission losses can be minimised. There are other advantages associated with PHEVs like petroleum usage becomes less for transport, lower charging costs at stations by usage of renewable energy sources, reduced greenhouse gases emission [2–5].

These PHEVs act as controllable loads or elastic loads in the system (G2V mode) as the charging restrictions are not stringent. Similarly, they can be used as power sources (V2G mode) with the same ease of control. For these reasons, it is estimated that there will be an exponential increase in the usage of PHEVs. The role of PHEVs and its popularity for the application in a smaller scale power system called microgrid is discussed in [6], where the power exchange was controlled by the aggregator of PHEVs by coordinated scheduling [7]. It is observed in the literature that the concept of aggregator as a single point of communication contact with the available fleet of PHEVs is the optimised way to handle and communicate with them.

In this paper, an aggregator receives the information of the number of PHEVs available for participation in the frequency regulation and their SOC levels are also communicated to the Central Controller (CC).

During frequency regulation, the power generation requirement changes dynamically and hence require robust, reliable and quick responses from sources. SPV has a special characteristic of higher ramp rate compared to any other renewables. Hence SPV can readily participate in load sharing during frequency regulation. ANN based and fuzzy based MPP detection was previously applied in this context for simulation and real-time experimentation [8–15].

Operation of the SPV under Maximum Power Point (MPP) is considered as a traditional approach to increase the efficiency of the source. SPV need not always operate at the MPP, but can lower its power output so that it can be a reserve in the system when needed. The modulation index of the converter, connecting SPV to grid, can be modified to increase or decrease the power output to participate in frequency regulation [17], where a Neuro-Fuzzy Controller (NFC) was applied to vary the power injection to the grid, eliminating the power storage requirements.

In this paper SPV is controlled by NFC for LPP operation while PHEV is applied in the V2G mode and it is assumed that batteries of vehicles are charged not from the grid but a separate source available at the charge stations available at households, offices, and commercial establishments dedicated for battery charging. An additive-adaptive algorithm is applied to have integrated operation of the sources and to maintain the system frequency within limits.

The rest of the paper is organised as follows. In Section 2, a brief description of the modelling of SPV, FC, DG and PHEV sources is discussed. In Section 3, the neuro-fuzzy control scheme used to control output of SPV is discussed in detail. In Section 4, the overall system interconnection where the role of CC and the Local Controller (LC) is described in detail. The various scenarios considered for testing the system performance along with the analysis of results are presented in Section 5. The conclusions for the work done is presented in Section 6.

2 SPV, FC, DG, PHEV Modelling

2.1 Solar PV Model

The diode model of the SPV [18] is represented with the following formulae

$$I_{PH} = [I_{SC} + K_I\,(T_{PV} - T_{REF})]\,H \tag{1}$$

$$I_{RS} = T_{R,REF}\left(\frac{T_C}{T_{REF}}\right)^3 \exp\left(\frac{q\,E_G}{kA}\left(\frac{1}{T_{REF}} - \frac{1}{T_C}\right)\right) \tag{2}$$

$$I_{PV} = N_{PARALLEL}\left(I_{PH} - I_{RS}\left(\exp\left(\frac{q}{k\,T_C\,A}\frac{V_{DC}}{N_{SERIES}}\right) - 1\right)\right) \tag{3}$$

Where I_{PH} is the photo current, I_{SC} is the short circuit current taken as 8.03 A, K_I is the temperature coefficient of the short circuit current is taken as 0.0017, T_{REF} is the reference temperature (298 K), H is the solar irradiation incident on the panel (W/M2), T_{PV} is the temperature of the panel. In Equation (2), the reverse saturation current of the cell is defined as a function of reverse saturation current reference $I_{R,REF}$ considered here as 1.2×10^{-7}, electron charge q (1.602×10^{-19} C), cells band gap energy level E_g (1.12), Boltzmann's constant (1.38×10^{-23} J/K), ideality factor A is taken as 1.92. Equations (1) and (2) can be substituted in Equation (3) where V_{DC} represents the DC output voltage, N_{SERIES} is the number of cells in series (1050), $N_{PARALLEL}$ is the number of strings in parallel (5) as in above equation.

The power output of the solar panel can be formulated as shown in Equation (4).

$$SPV_{POWER} = V_{DC} * I_{PV} \tag{4}$$

2.2 Fuel Cell Model

It is an electro-chemical device converting hydrogen and oxygen into water along with free electrons which results in a direct-current electricity production. Fuel cells are gaining attention and are being extensively used because of its advantages like high efficiency wide fuel range, modularity and ease of logistics [19]. FC system consist of two main parts. They are a) Reformer and b) Stack.

2.2.1 Reformer

It produces hydrogen gas from various fuels like carbohydrates and gives it to stack. Reformer can be considered as a RC network as shown in Figure 1.

The First order transfer function representation with larger time constant can be written as shown in Equation (5).

$$\frac{V_{cr}}{V_{in}} = \frac{1}{1 + \tau_r\, S} \tag{5}$$

Where V_{in} and V_{cr} are the input and output voltages, R_r and C_r are the Resistive and Capacitive elements of the network and $\tau_r = R_r * C_r$ is the time constant of reformer.

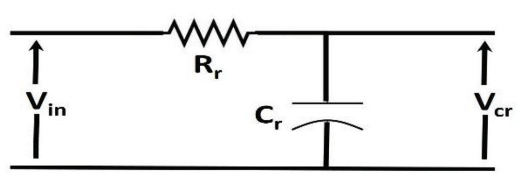

Figure 1 RC Network approximation of Reformer in FC.

2.2.2 Stack

Stack takes hydrogen from the reformer and passes it through the set of unit-cells consisting of electrolyte separation and plates. Here stack is electrically modelled as

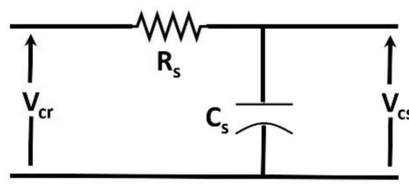

Figure 2 RC Network approximation of Stack in FC.

The transfer function of model is written as

$$\frac{V_{cs}}{V_{cr}} = \frac{1}{1 + \tau_s\, S} \tag{6}$$

Where V_{cr} is the output of reformer and V_{cs} is the stack output voltage, R_s and C_s are the Resistive and Capacitive elements of the network, τ_s = R_s*C_s called time constant of the stack. It is always considered that $\tau_r > \tau_s$.

The modelling of the hydrogen and oxygen tanks, fuel utilization, the demand current limits, input fuel control, time response and the parameters are as mentioned in [20].

2.3 Diesel Generator Model

The block diagram representation of DG is a combination of three parts namely fuel rack actuator, combustion process and the rotor speed transfer functions [20]. Controlling the valve of the actuator initiates controlled change in the mechanical output of the engine. The output rotational mechanical energy is given as an input to the generator, thus getting the desired level of electrical power output. This combination can further be approximated as a simple first order transfer function, as shown in equation

$$\frac{\Delta P_{DG}}{\Delta F} = \frac{K_{DG}}{1 + T_{DG}\, S} \tag{7}$$

2.4 PHEV Battery Model

PHEV is a combination of two power stages. One with an IC engine mechanically connected to the rotor of generator and the other, a battery pack with high energy storage capability. Each battery is having a charging or discharging current rating (C) in terms of one-hour capacity. Depending on the battery's Discharge curve, the State-of-charge decreases proportionately [22]. This SOC is an important parameter in estimating the available capacity in terms of actual capacity of the battery. [23] shows the electrical equivalent model of the battery, considering the chemical reactions inside, with the internal elements E and Z as a function of SOC. The vehicle batteries are considered getting charged at a station with dedicated power sources, except the microgrid. When the PHEV shows willingness to participate in load sharing, the SOC is calculated based on the open-circuit voltage and temperature. Since the vehicle is supposed to travel a minimum distance, there will be minimum limits declared for the SOC, below which, the battery should get disconnected from pumping power into the grid. In this paper, it is estimated that a minimum of 25% SOC is required to drive back home.

3 Limited Solar Power Point Tracking Using Neuro-Fuzzy Controller (NFC) for a Storage Free System

3.1 System Power Reserve and LPP Tracking Operation

Traditional operation of SPV needs a controller to track the Maximum Power Point (MPP) so that maximum efficiency is achieved. To make SPV act as a reserve it is necessary to operate it at less than its MPP [17]. The neural network is designed to take feedback of power output of the SPV and the

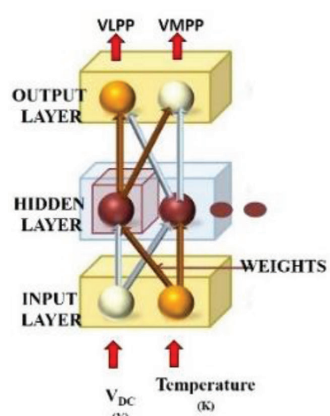

Figure 3 Neural Network structure schematic considered.

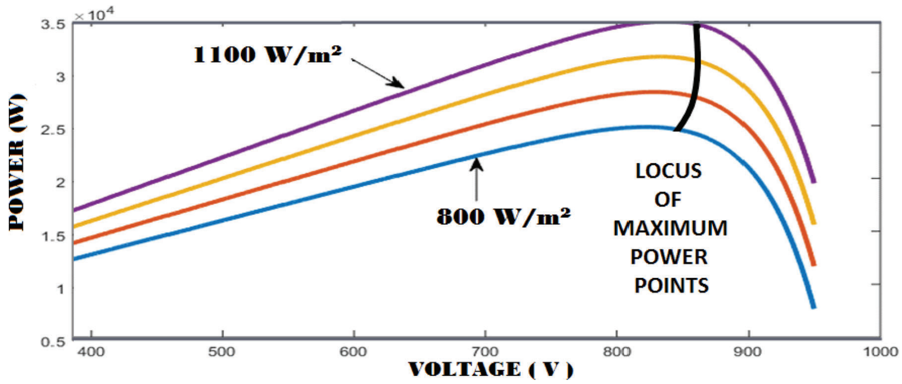

Figure 4 SPV Power versus Voltage and locus of MPPs for varying insolations.

temperature of the panel as inputs to estimate the voltage at which the LPP operation for a set-point reserve is obtained and the voltage for MPP operation.

The neural network is trained based on rigorous testing of SPV system described in Section 2.1. The MPP in each case of varying insolation levels are found and a locus of those points are mapped. In Figure 5, the variation of locus of MPPs for various temperatures is shown. This data is again consolidated for varying temperature, V_{MPP}, varying insolation and Power at MPP. The resulting graph is shown in Figure 6.

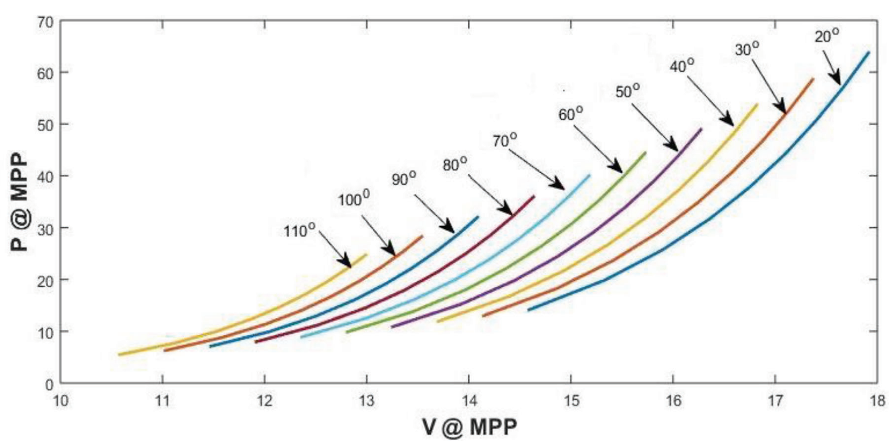

Figure 5 Variation of loci of MPPs as temperature of the panel changes.

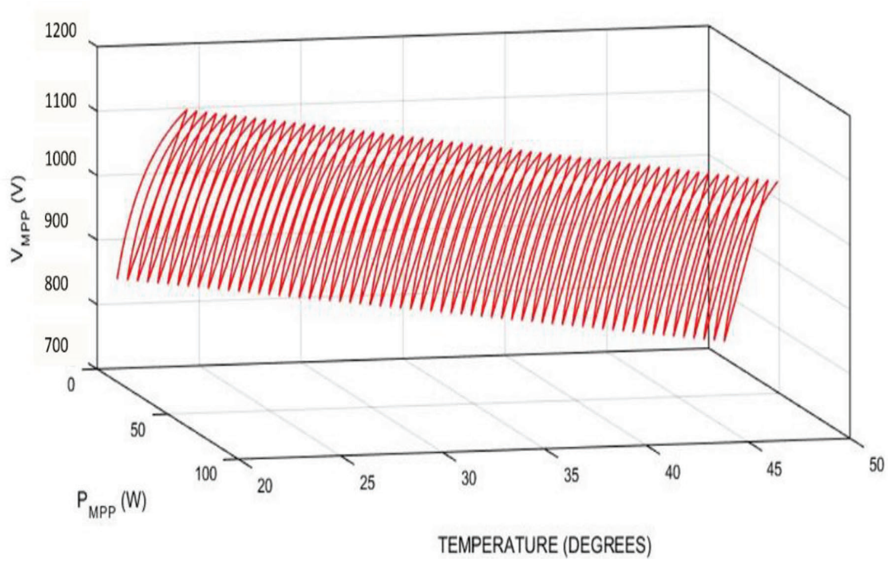

Figure 6 Consolidation of variation of V_{MPP} values as P_{MPP} changes with respect to temperature, training data for neural network.

More than twelve thousand samples are used to train, validate and test the neural network in the ratio of 14:3:3 respectively for its realization in the present form.

3.2 Neuro-Fuzzy Controller

The overall SPV system considered in this paper is shown in Figure 7. The output of Equation (3) is realized and compared to the feedback signal of DC current fed into the grid. This signal is converted into the voltage signal, modelled by a capacitor link. The difference between actual voltage developed and the reference is given to the PI controller and the transfer function approximation of the SPV. The neuro fuzzy controller decides the $V_{dc,ref}$ value so that the system operates at desired LPP.

3.3 Fuzzy Controlled DC Voltage Reference Setting

The operating region is considered on the right side of the MPP in Power versus voltage graph of SPV [17]. The range of operation is between the MPP and Zero Power Point (at open-circuit-voltage). Depending on the scale of deviation of frequency DelF, the reference point of DC Voltage given to the

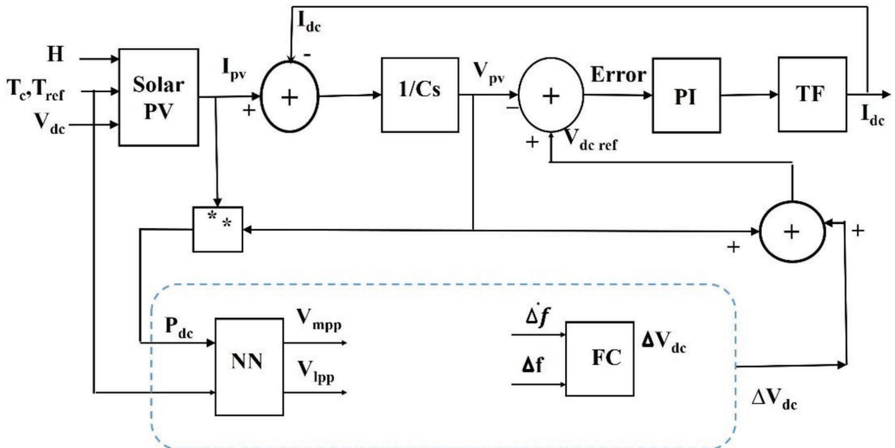

Figure 7 Overall SPV system design.

SPV's PI controller must be changed to shift the operating point upwards or downwards. The derivative of the feedback DelF is taken to understand the rate of change of error and used as an input to fuzzy logic controller, while the other input is DelF. The crisp values are fuzzified into and defuzzified from five categories of membership functions each, namely Big Negative (BN), Small Negative (SN), Zero (Z), Small Positive (SP) and Big Positive (BP). Among these, BN and BP are taken as trapezoidal membership functions and others as triangular membership functions. The details of the membership function parameters used are furnished in [17]. Mamdani type of system is used and centroid method of defuzzification is applied in this paper. The rule base and the truth table for mapping inputs and outputs is shown in Figure 8.

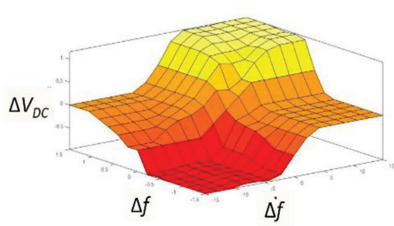

(a)

RULE BASE		$\dot{\Delta f}$				
		BN	SN	Z	SP	BP
Δf	BN	BN	BN	SN	SN	Z
	SN	BN	SN	SN	Z	SN
	Z	SN	SN	Z	SN	SN
	SP		Z	SN	SN	BP
	BP	Z	SN	SN	BP	BP

(b)

Figure 8 (a) Surface view of rules considered for fuzzy logic controller (b) Rule-table for rules between Δf, change in Δf and output ΔV_{DC}.

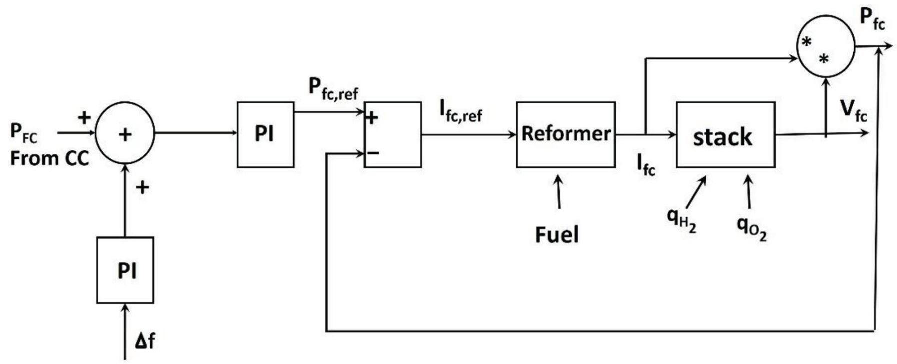

Figure 9 Overall FC system design.

4 System Description and Adaptive-Additive Strategy (AAS) based Control Algorithm

4.1 Overall System Description

The system considered in this paper consists of DG, SPV, FC and PHEV. DG is always committed first to serve the critical and sensitive loads in the system, which account to 0.1 pu. So, the minimum generation of diesel is 0.1 pu, while the maximum generation possible is 0.5 pu. SPV has a maximum capacity of 0.29 pu, of which, always a reserve of 10% is maintained when there is 100% insolation available. Fuel cell can play its part with a maximum penetration level of 0.5 pu. The PHEV's power availability is based on a) availability of the vehicle for discharging b) SOC levels of the vehicle battery. In this paper five PHEVs are assumed to be available during the time of simulation with different SOC levels, each contributing a maximum of 0.1 pu of power discharge. The block diagram representation of the system described is shown in Figure 10.

The CC installed in the microgrid manages the real power flow between the generators to the load. The unit commitment and load dispatch is done based on order of priority i.e., DG, SPV, FC, PHEV. The difference between sum of power generated and load is applied to the drooping characteristics representing the microgrid system to understand the frequency change (DelF) in the system. This DelF is taken as a feedback and given to the local controllers (PI) present at the generator site, to make proportionate changes in power generation (represented by blue dotted lines). PHEVs are not a part of the frequency regulation as the response time is greater than that of the power system's response.

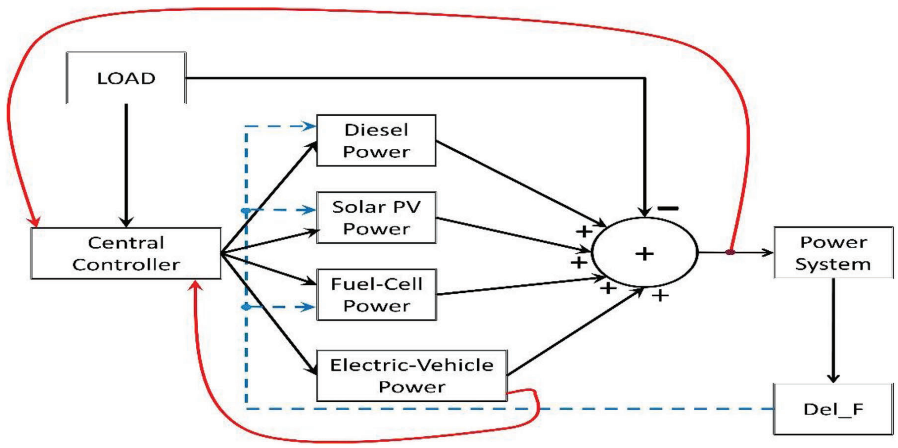

Figure 10 Block diagram representation of power system considered.

4.2 AAS Control Strategy

There are two types of controllers employed in the system. One, operating at a central level and others acting locally at the generator site. The Central Controller (CC) mainly works on the commitment of units to match the load requirement. The frequency error is directly sent to the local controllers to make necessary adjustments.

4.2.1 Central controller

The CC receives inputs mainly from the load prediction centre, where demand is estimated for the next minute. The allocation of power for each generator is decided dynamically on priority basis. As already mentioned, DG will meet the critical load demand and generation of 0.1 pu is a mandate for these loads. SPV shall operate at LPP and hence the local controller at SPV needs a command of increase or decrease in the reference value along with the share of SPV power to be generated. FC is targeted next for sharing the load demand. The information of availability, minimum and maximum levels is communicated at the start of the day based on tank volume and pressure conditions. As a last option, PHEVs are involved in load sharing. The information of how many vehicles are available and their battery SOC levels are communicated with CC. Depending on the SOC levels, EVs are committed in order of priority. As the vehicle is under discharge mode, its SOC levels are continuously evaluated using the formula

$$SOC = 100\left(1 - \frac{1}{C}\int_0^t i(t)\right)\% \tag{8}$$

Where C represents the ampere hour capacity rating of the battery, $i(t)$ is the current discharged at time t.

The information of whether there is any difference between the estimated load and actual load, either because of load variation or load not met, is obtained as a feedback. Based on the scale of deviation, two types of control actions are initiated. The flowchart shown in Figure 11 explains the action taken. The approach is called additive-adaptive nature based because, initially the CC allocates load sharing on additive basis and the DelF command initiate adaptiveness in the algorithm.

CC also receives signals from PHEV station regarding the availability of vehicle for load sharing and its SOC levels. In this paper, it is assumed that all the PHEVs are having the same battery type and ratings for simplicity. The charge controller collects energy from vehicle's batteries based on the CC commands. It calculates the difference between load and total generation, after committing DG (0.1 pu), SPV (at LPP) and FC, taking required energy from batteries committed with respective discharge rates.

4.2.2 Local controllers

4.2.2.1 *SPV- NFC*

As mentioned in Section 3, the fuzzy controller receives command from the feedback, indicating the change in frequency of the system. SPV is carefully operated between the LPP of 90% MPP and below, unless clearance is given from CC to operate at MPP. One such scenario is considered in the next section.

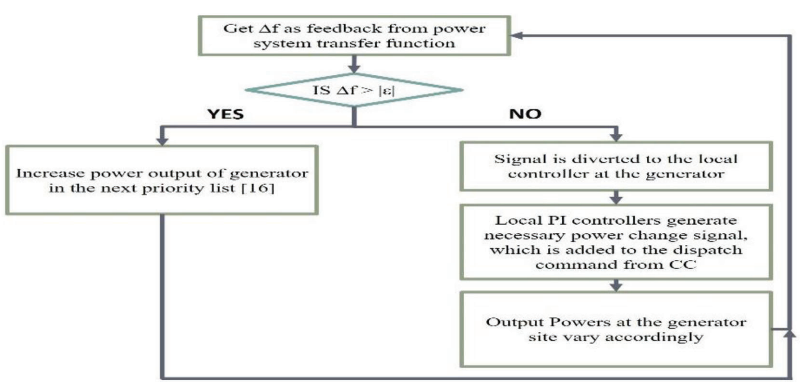

Figure 11 Algorithm followed by CC as a response to frequency change in the system.

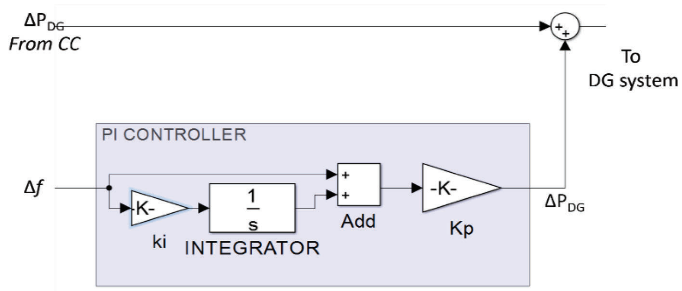

Figure 12 Proportional-Integral Controller of DG.

4.2.2.2 *DG Proportional-Integral controller*

The response of DG is usually slow and hence in most of the cases, the ease of participation in load sharing for frequency regulation by DG is comparatively slow. There is also a limit on the negative power change request command if present, to protect the critical loads. In this paper load sharing from 0.1 pu to the maximum of 0.5 pu is allowed. The schematic of the controller used is shown in Figure 12. A traditional Proportional Integral (PI) controller is employed to understand the frequency error in terms of power change request command. The K_p and K_i values considered here are taken from the appendix of [17] as 1500 and 10 respectively.

4.2.2.3 *FC Proportional-Integral controller*

A similar kind of a PI controller shown in Figure 12 is also used for fuel cell power output control. The output of the controller is added to the command from CC to ensure that the difference between predicted and actual load is met during transient and steady state operations of the system.

5 Scenarios Considered and Analysis of Performance

The analysis of the system is done by considering various cases/scenarios under which the system response must be studied for the frequency variation from its nominal value of 50 Hz. In the following subsections, four scenarios are discussed based on increasing load demand and varying solar insolations.

5.1 Scenario – 1

Assuming solar insolation levels are 100% and there are enough reserves of diesel, hydrogen and oxygen, load is starting from 0.8 pu and reaching a peak of 0.95 pu during the 240-sec simulation time, changing in steps for every 50 sec. The system starts from zero initial state and hence a frequency error of about 0.2 Hz. Initially DG is asked to deal with critical loads accounting to 0.1 pu. SPV straightaway contributes the maximum minus the reserve capacity of 10%. FC contributes remaining power. Between 50–110 seconds, FC steps up its generation to match the load. For the next step load change, load increases beyond the capacity of FC and hence Power Request Command (PRC) is sent to PHEV. The remaining demand is now delivered by the vehicle having the highest SOC among the available PHEVs. This is explained in Figure 13. The second EV discharges the power in accordance with PRC obtained from the controller. Other vehicles remain idle, not participating in the frequency regulation. The frequency error can be observed to be within the allowable band of ± 0.05 Hz by the action of coordinated control of central and local controllers. At 200$^{\text{th}}$ second, when there is a step load decrease, as per the priority order, PHEV reduces its power delivery to the system as shown in Figure 14. The following observations can be made from the results a) ones the frequency error DelF comes into the bracket of allowable range (indicated with dotted lines), whether there is a positive or negative step load change, the controllers and the generators can respond quickly to keep frequency intact.

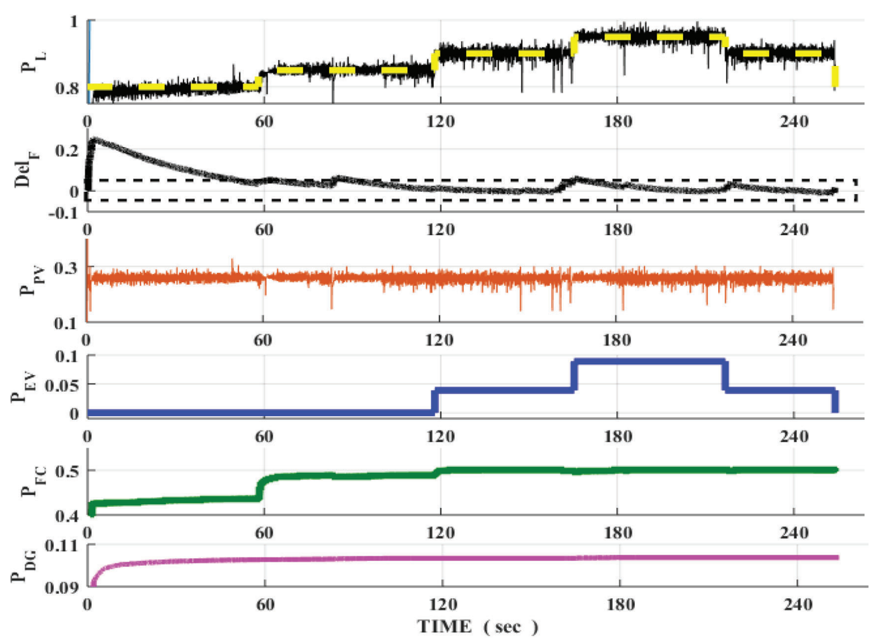

Figure 13 DG, FC, EV, SPV response for load sharing, frequency error and load considered.

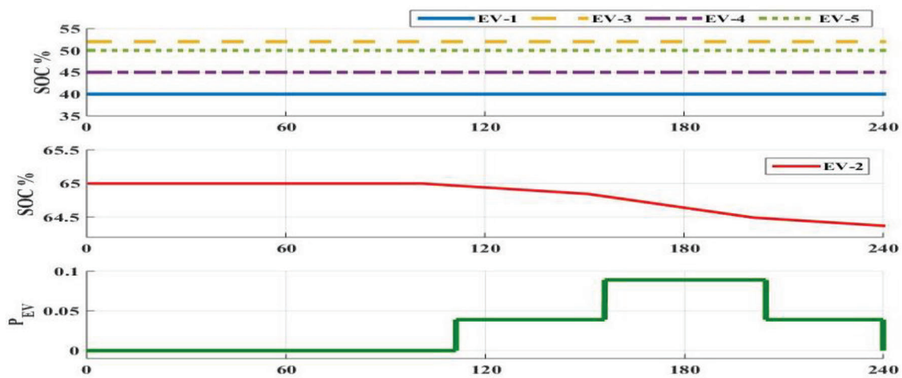

Figure 14 Load sharing of PHEVs and associated SOCs of respective vehicle batteries versus time.

b) PHEVs are responding based on SOC available. c) The neuro-fuzzy controller can maintain the SPV to deliver 90% power, under varying load conditions. d) Between 110–240 seconds the discharging rates of PHEV-2's battery, change in accordance with the PRC signal obtained from the controllers. According to the droop characteristics (ΔF vs ΔP), for every Δ change in load demand, there is a change in system frequency as mentioned in appendix of [17]. This change in frequency command is given to the main and local controllers which inturn generate a power change request. Therefore, there will be an increase or decrease in power generation by any of the distributed generation sources considered based on the PRC signal. The typical time taken by the controllers for every 0.01 pu of PRC is 5s for DG, 3s for FC and 0.5s for SPV and PHEVs.

5.2 Scenario – 2

In this case, load considered varies from 1.2 pu to 1.35 pu. As usual, DG initially is contributing 0.1 pu for critical load, SPV takes up LPP operation, Fuel cell hits its maximum of 0.5 pu. Hence PHEV starts discharging power into the grid to match the demand. PRC shall be sent to PHEVs based on pu requirement of the system, analysed by the controller. When the load hits 1.35 pu, instead of sending small negative PRC ($1.35_{\mathrm{LOAD}} - 0.265_{\mathrm{SPV}} - 0.1_{\mathrm{DG}} - 0.5_{\mathrm{FC}} - 0.5_{\mathrm{PHEV}} = -0.015$ PU) to PHEVs, FC takes the correction, as it is easy to regulate flow of oxygen and hydrogen than to send a request to vehicle site. This can be observed in Figure 15. The DG is serving only the critical loads as the total load required is met by other sources.

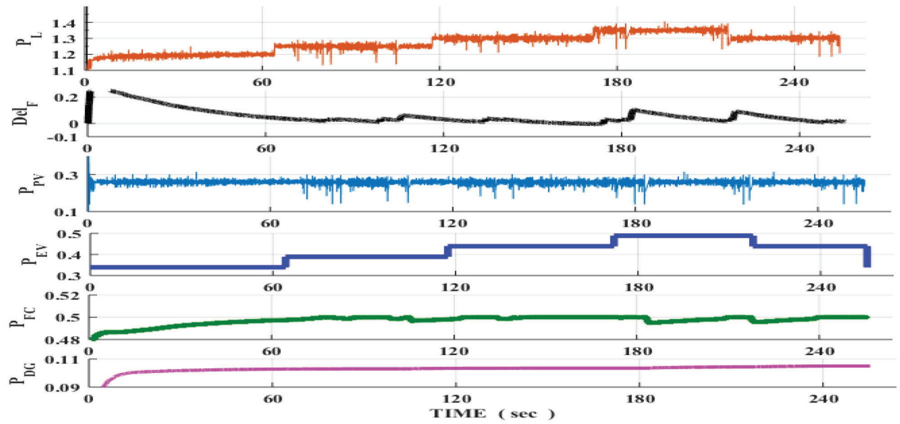

Figure 15 DG, FC, EV, SPV response for load sharing, frequency error and load considered.

5.3 Scenario – 3

Here, the system is operated in a load range of 1.4 pu to 1.55 pu, close to the maximum capacity of the system. The performance of the system is shown in Figure 16. Starting at a value of 1.4 pu, SPV, FC, PHEV are delivering at their upper-limits, with reserve available. the SOCs of the five PHEVs considered here are {50 30 60 30 60} in percentages. Since the PRC required is equal to max. capacity of the battery bank available, the power is delivered by all the batteries and at equal discharge rates. The second and fourth batteries hit their minimum SOC level of 25% at around 60th second. Hence, they shall be excluded from power sharing. Now the available power from PHEVs is only 0.3 pu. At 310th second 1st PHEV and at 450th second, remaining third and fifth PHEV's SOC levels also drop to the minimum acceptable levels. This can be clearly observed in Figure 17. Meanwhile, at 340th second, for a step load of +0.1, DG, FC and PHEV are delivering at maximum levels. Hence, SPV picks up from its LPP to MPP value, bringing the reserve power of 10% into picture. Further raising of load is shed off, since further power generation is not possible. At 451st second, further load shedding takes place as PHEVs are not participating in the load sharing. Following observations can be made from the results a) as the load increases, the time taken by the frequency error DelF to reach acceptable limit increases because of the system's response. b) The frequency variation is limited between the limits of ± 0.1 Hz, the average being close to zero. c) Care is taken not to shed the critical loads. d) The PLOAD graph shows that the load met (blue line) is closely related to the actual load (white dotted line) shown in the Figure 16.

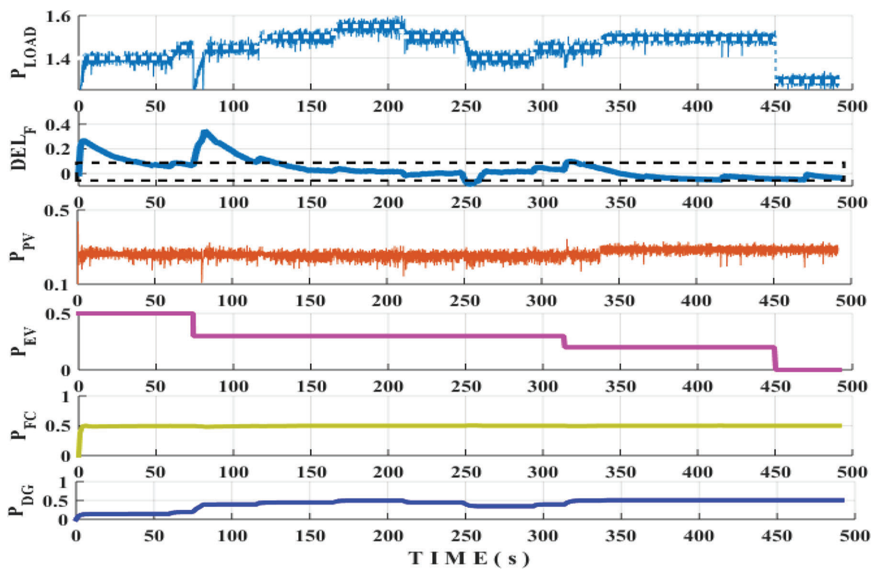

Figure 16 DG, FC, EV, SPV response for load sharing, frequency error and load considered.

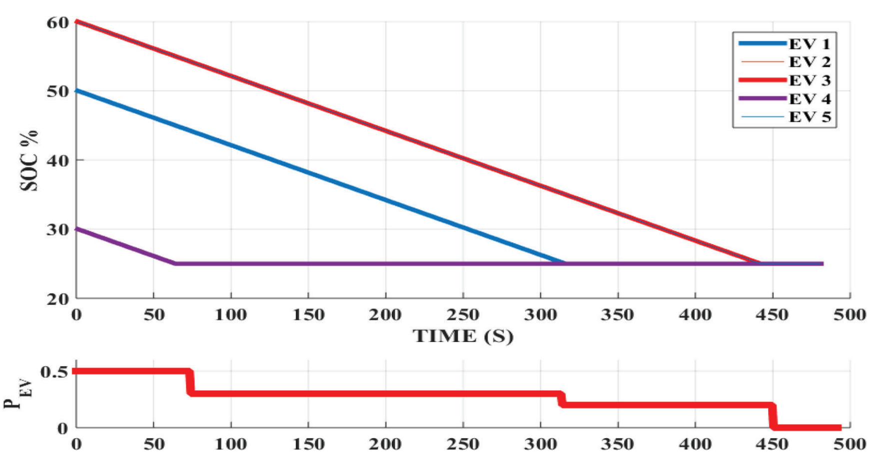

Figure 17 Load share of PHEVs and associated SOCs of respective vehicle batteries.

5.4 Scenario – 4

The solar irradiation levels are meant to change over the available day time. In this scenario, we consider irradiation variation from 70% to 30% of nominal value (1000 W/m^2), shown in Figure 18. From 0–150 seconds, irradiation is around 70%. During this period, it can be observed that the load varies every

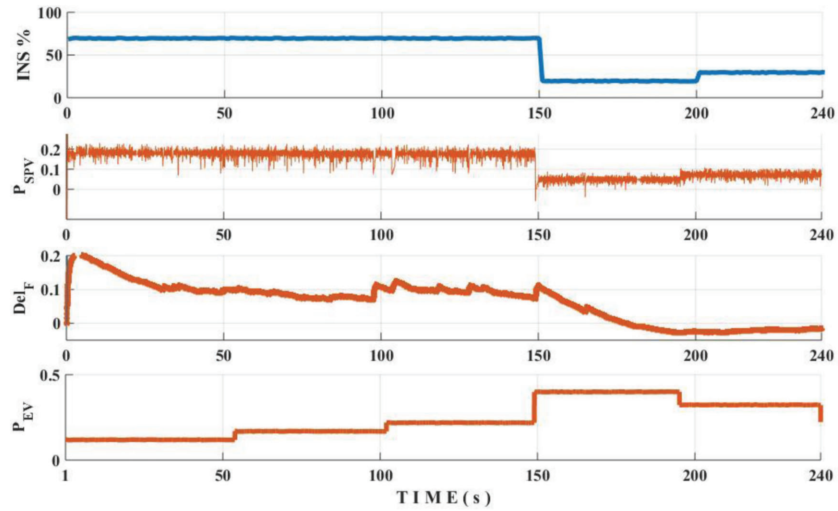

Figure 18 Change in insolation levels, Change in frequency (Hz), SPV and PHEV output powers (pu).

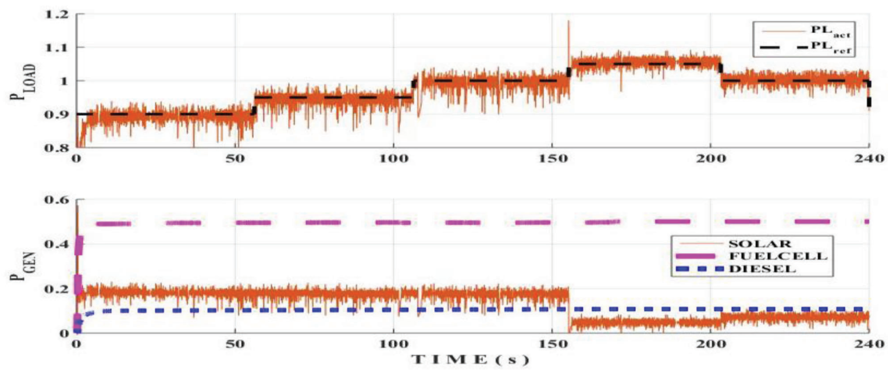

Figure 19 Load met and the power dispatch between the generators under varying insolation conditions.

50 seconds. Solar power is delivered at a constant rate, proportional to the insolation levels i.e., around 0.2 pu. After 150th second, insolation level drops to around 20%. The SPV output can also be seen to lower proportionally. The neuro-fuzzy local controller operates at LPP, maintaining reserve capacity. PHEVs participating in the load share take the burden of decrease in the SPV output especially after 150th second. The DelF is maintained between

the acceptable limits by the controllers using a coordinated approach. From Figure 19, the response of FC, DG and the load met by the system can be analysed. FC is delivering at its maximum value, while DG is meeting the critical load demand. The graph of actual load met shows that system is acting as a path follower of requested load demand. This concept of varying insolations can be tested along with the above scenarios. It is found to be giving a satisfactory range of frequency variation within the limits. Description of it in this paper is beyond the scope and left to the reader.

6 Conclusion

In a microgrid environment where the system is equipped with SPV, DG, FC and PHEVs, frequency regulation must be maintained under varying load conditions (in steps) maintaining a reserve capacity without energy storage system included in the system. In this paper, various scenarios have been considered for testing the system and results show the successful implementation of a simple additive-adaptive based strategy. The coordinated operation of the sources under the PHEV SOC limits is also observed from the analysis.

Acknowledgement

We would like to thank IIT Delhi, India for providing fellowship under Quality Improvement Program to facilitate research work and CVRCE for permitting us to carry out the work.

References

[1] Kempton, W., and Tomić, J. (2005). Vehicle-to-grid power fundamentals: calculating capacity and net revenue. *J. Power Sources* 144, 268–279.
[2] Minnesota Pollution Control Agency (2007). *Air Emissions Impacts of Plug-In Hybrid Vehicles in Minnesota's Passenger Fleet*. St. Paul, MN: Minnesota Pollution Control Agency.
[3] Graham, R. (2001). *Comparing the Benefits and Impacts of Hybrid Electric Vehicle Options*. Palo Alto, CA: EPRI.
[4] EPRI (2002). *The Benefits and Impacts of Hybrid Electric Vehicle Options for Compact Sedan and Sport Utility Vehicles*. Palo Alto, CA: EPRI.
[5] Yokoyama, A. (2010a). Smarter grid I. *IEEJ J*. 30, 94–97.
[6] Yokoyama, A. (2010b). Smarter grid II. *IEEJ J*. 30, 163–167.

[7] Yokoyama, R., Hida, Y., Koyanagi, K., and Iba, K. (2011). "The role of battery systems and expandable distribution networks for smarter grid," in *Proceedings of the IEEE Power and Energy Society General Meeting* (Detroit, MI: IEEE), 1–6.

[8] Han, S., Han, S., and Sezaki, K. (2010). Development of an optimal vehicle-to-grid aggregator for frequency regulation. *IEEE Trans. Smart Grid* 1, 65–72.

[9] Esram, T., and Chapman, P. L. (2007). Comparison of photovoltaic array maximum power point tracking techniques. *IEEE Trans. Energy Convers.* 22, 439–449.

[10] Hohm, D. P., and Ropp, M. E. (2000). "Comparative study of maximum power point tracking algorithms using an experimental, programmable, maximum power point tracking test bed," *Proceedings of the 28th IEEE Photovoltaic Specialists Conference*, Anchorage, 1699–1702.

[11] Hiyama, T., and Kitabayashi, K. (1997). Neural network based estimation of maximum power generation from module using environmental information. *IEEE Trans. Energy Convers.* 12, 241–247.

[12] Hiyama, T., Kouzuma, S., Imakubo, T., Ortmeyer, T. H. (1995). Evaluation of neural network based real time maximum power tracking controller for PV system. *IEEE Trans. Energy Convers*. 10, 543–548.

[13] Hiyama, T., Kouzuma, S., and Imakubo, T. (1995). Identification of optimal operating point of PV modules using neural network for real time maximum power tracking control. *IEEE Trans. Energy Convers*. 10, 360–367.

[14] Torres, A. M., Antunes, F. L. M., Reis, F. S. (1998). "An artificial neural network-based real time maximum power tracking controller for connecting a PV system to the grid," in *Proceeding of IEEE, the 24th Annual Conference on Industrial Electronics Society*, Vol. 1, Aachen, 554–558.

[15] Samangkool, K., and Premrudeepreechacharn, S. (2005). "Maximum power point tracking using neural networks for grid-connected photovoltaic system" in *Proceedings of the 2005 International Conference on Future Power Systems*, Amsterdam, 4.

[16] Masoum, M. A. S., and Sarvi, M. (2005). A new fuzzy-based maximum power point tracker for photovoltaic applications. *Iran. J. Electr. Electron. Eng*. 1, 28–35.

[17] Senjyu, T., Uezato, K. (1994). "Maximum power point tracker using fuzzy control for photovoltaic arrays," in *Proceedings of the IEEE International Conference on Industrial Technology,* Seville, 143–147.

[18] Sekhar, P. C., Mishra, S., and Member, S. (2015). Storage free smart energy management for frequency control in a diesel-PV-fuel cell-based hybrid AC microgrid. *IEEE Trans Neural Netw Learn Syst*. 27, 1–15.
[19] Yazdani, A., et al. (2011). Modelling guidelines and a benchmark for power system simulation studies of three-phase single-stage photovoltaic systems. *IEEE Trans. Power Del*. 26, 1247–1264.
[20] Kim, Y.-H., and Kim, S.-S. (1999). An electrical modelling and fuzzy logic control of a fuel cell generation system. *IEEE Trans. Energy Convers*. 14, 239–244.
[21] Zhu, Y., and Tomso, K. (2002). Development of models for analysing the load-following performance of microturbines and fuel cells. *Electr. Power Syst. Res*. 62, 1–11.
[22] Elmitwally, A., and Rashed, M. (2011). Flexible operation strategy for an isolated PV-diesel microgrid without energy storage. *IEEE Power Energy Soc*. 26, 235–244.
[23] Affanni, A., Bellini, A., Franceschini, G., Guglielmi, P., and Tassoni, C. (2005). Battery choice and management for new-generation electric vehicles. *IEEE Trans. Ind. Electron*. 52, 1343–1349.
[24] Ceraolo, M. (2000). New dynamical models of lead-acid batteries. *IEEE Trans. Power Syst*. 15, 1184–1190.

Biographies

K. S. V. Phani Kumar is a Ph.D. student in Jawaharlal Nehru Technological University, India since Nov 2012. He has specialized in Power systems during his master's studies at SRM University. He completed his Bachelor's degree in Electrical and Electronics from Anna University and his M.E from S.R.M University Chennai. He is currently working for in the areas of Distributed Generation, Optimization techniques and Power Quality in Microgrids. He is presently working as Assistant Professor in the department of Electrical and Electronics Engineering at CVR College of Engineering, Hyderabad, India.

S. Venkateshwarlu Completed his B.Tech from Sri Venkateshwara University, Tirupati in Electrical & Electronics Engineering, Masters from NIT Waranagal with Electrical Machines & Industrial Drives specialization, Kakatiya University and Ph.D from College of Engineering, Osmania University, Hyderabad in 2011. His areas of interests are Power Electronics, FACTS applications and Power quality. He is currently working as Professor & Head of Electrical and Electronics Engineering at CVR College of Engineering, Hyderabad, India.